Journal of Materials Chemistry B

PAPER

Cite this: J. Mater. Chem. B, 2014, 2, 7201

Facile synthesis of functional gadolinium-doped CdTe quantum dots for tumor-targeted fluorescence and magnetic resonance dual-modality imaging

Fei Zhang,[a] Ting-Ting Sun,[a] Yan Zhang,[b] Qiong Li,[c] Chao Chai,[c] Li Lu,[c] Wen Shen,[c] Jun Yang,[b] Xi-Wen He,[a] Yu-Kui Zhang[ad] and Wen-You Li*[a]

Received 6th June 2014
Accepted 14th August 2014

DOI: 10.1039/c4tb00920g

www.rsc.org/MaterialsB

Magnetic quantum dots (MQDs) are an important class of agents for fluorescence (FL)/magnetic resonance (MR) dual-modal imaging due to their excellent optical and magnetic properties. However, functional MQDs prepared by a simple room-temperature route as FL/MR dual-modal imaging probes are lacking. Herein, we report the fabrication of Gd-doped CdTe quantum dots (Gd:CdTe QDs) as an agent for FL/MR dual-modality imaging. The as-designed QDs with an ultrasmall particle size are synthesized by a facile one-pot aqueous synthesis approach at room temperature. They emit strong fluorescence at 640 nm with a quantum yield of 37% in water, and they have a high longitudinal relaxation rate (r_1) value of 3.27 mM^{-1} s^{-1}. With the further conjugation of folic acid, the Gd:CdTe QDs can successfully label live HepG2 cells for targeted cellular imaging and present no evidence of cellular toxicity up to the concentration of 0.5 mg mL^{-1}. They have been employed as a suitable contrast agent successfully for tumor-targeted FL/MR dual-modal imaging in a mouse model.

1. Introduction

In recent years, semiconductor nanocrystals or quantum dots (QDs) have attracted intense research interest in biomedical imaging applications due to their unique optical properties caused by quantum confinement.[1–11] Compared with the traditional organic dyes, QDs have several advantages, including broad excitation spectra,[6] narrow emission spectra,[9] large Stokes shift,[12] high quantum yield (QY),[5,13] high resistance to photobleaching,[6,9] excellent water solubility and biocompatibility.[12–14] These advantages make them an alternative to play an important role in fluorescence imaging (FI) technique, which can afford high sensitivity, high spatial resolution, target specificity and real-time imaging at cellular level for disease diagnosis and other applications.[7,15]

However, FI technique also has its own disadvantages, such as low tissue penetration depths[16–18] and the disturbance of autofluorescence,[19,20] which restricts its application in deep tissue imaging.[16–21] In contrast, magnetic resonance imaging (MRI) is a non-invasive imaging technique without ionizing radiation, which can provide more outstanding tissue penetration depth and higher resolution of anatomy, but lower sensitivity than FI.[15] As a result, the probes that simultaneously contained the response ability of FI and MRI have been designed and fabricated in order to gather the merits of each imaging modality and increase the accuracy of imaging results.[22–31]

As a significant type of agent for FI/MRI dual-modal imaging, magnetic ions-doped quantum dots (MDQDs) can integrate both optical and magnetic capabilities in a single nanoparticle. Compared with the other FI/MRI agents based on QDs and magnetic materials, such as composite particles,[23] core/shell or heterostructures of QDs and magnetic materials[24] and QDs with a paramagnetic coating of Gd-chelates,[24,32] MDQDs have a smaller particle size, which is not only suitable for cellular imaging, but also increases the clearance of the agents from the body.[32–35] On the other hand, MDQDs can avoid damage to the fluorescence property of QDs probes, which is caused by the nonradiative capsulation materials in some composite particles or core/shell agents.[24,25] Furthermore, most MDQDs can be prepared by a one-step strategy.[19–24] This synthesis strategy also affords a cost-effective synthesis approach by reducing the reaction steps and the waste of reagents.

[a]State Key Laboratory of Medicinal Chemical Biology (Nankai University), Collaborative Innovation Center of Chemical Science and Engineering (Tianjin), and Research Center for Analytical Sciences, College of Chemistry, Nankai University, 94 Weijin Road, Tianjin 300071, P. R. China. E-mail: wyli@nankai.edu.cn

[b]State Key Laboratory of Medicinal Chemical Biology and The Key Laboratory of Bioactive Materials (Ministry of Education), College of Life Science, Nankai University, 94 Weijin Road, Tianjin 300071, P. R. China

[c]The First Central Clinic College, Tianjin Medical University, and Department of Radiology, Tianjin First Central Hospital, 24 Fukang Road, Tianjin 300192, P. R. China

[d]National Chromatographic Research and Analysis Center, Dalian Institute of Chemical Physics, Chinese Academy of Sciences, Dalian 116011, China

For these reasons, more and more MDQDs, such as, Gd-doped ZnO QDs,[7] Ni-doped CdTeSe/CdS QDs,[13] Fe-doped CdTeS QDs,[22] Gd-doped CdSe QDs,[24] Mn-doped CdSe QDs,[36] Mn-doped CdS/ZnS QDs[37] and Gd-doped Eu_2S_3 QDs, have been established as dual-modal agents in the last two decades.[38] There are many reports on the fabrication of MDQDs, but few described aqueous synthesis of doped quantum dots. In 2010, Yeh *et al.* prepared Gd-doped CdSe QDs for FI/MRI *via* a hot injection approach in *n*-tetradecylphosphonic acid/trioctylphosphine oxide (TDPA/TOPO) solution at a high temperature of 280 °C.[24] This synthesis in organic phase needs a surface modified process or a phase-translation process to enhance the water solubility and biocompatibility of the QDs, which may significantly reduce the quantum yield (QY) of the QDs and cost more reagents and energy.[39] Although Fe-doped CdTeS QDs can be synthesized by a simple hydrothermal method without any organic solution, high temperature (180 °C) is also necessary for the reflux process.[22] Therefore, establishing an aqueous route for preparing MDQDs at low temperature is an appealing topic for synthesizing MDQDs.[40–42]

Here, we developed Gd-doped CdTe (Gd:CdTe) QDs as a dual-modality imaging agent for FI/MRI by a facile, one-pot, room-temperature strategy in aqueous solution without N_2 protection, pH adjustment and reflux process. The as-prepared Gd:CdTe QDs exhibit ultrasmall particle size, little cellular toxicity, high biocompatibility and a high QY. Since a Gd^{3+} ion has a symmetric electronic ground state and a high magnetic moment that is caused by the seven unpaired electrons in it,[8,43,44] the as-prepared Gd:CdTe QDs also show excellent paramagnetic property.

In order to increase the tumor-targeting capability of the Gd:CdTe QDs, we conjugated folic acid (FA) on the surface of the Gd:CdTe QDs by an EDC/NHS coupling method.[45,46] With the further conjugation of FA, the doped QDs were used for bioimaging application and exhibited outstanding tumor-targeted fluorescence imaging ability both *in vitro* and *in vivo*. Moreover, it was also successfully used as a probe for magnetic resonance imaging.

2. Experimental section

2.1. Materials

$CdCl_2 \cdot 2.5H_2O$ (98%+), glutathione (GSH, 99%+), $Na_2TeO_3 \cdot xH_2O$ (99%+), $NaBH_4$ (98%+), dimethyl sulfoxide (DMSO, 99%), 3-(4,5-dimethyl-2-thiazolyl)-2,5-diphenyl-2*H*-tetrazolium bromide (MTT, 98%), folic acid (98%+), carbodiimide (EDC, 98%), *N*-hydroxysuccinimide (NHS, 98%), PBS buffer solution (20×) and $N_2H_4 \cdot H_2O$ (80%) were purchased from J&K Scientific Ltd., China. $GdCl_3 \cdot xH_2O$ (98%+) was purchased from Alfa Aesar, China. All stock solutions of chemicals were prepared in deionized water, which was obtained from an AWL-0502-U super pure water system (Aquapro, China). All reagents were used without further purification.

2.2. Cells and animals

HepG2 cells were purchased from College of Life Science, Nankai University, Tianjin, P. R. China. The cells were cultured at 37 °C and with 5% CO_2 in Dulbecco's modified Eagle's medium (DMEM) supplemented with 10% fetal bovine serum (FBS). "Balb/c nude" mice and "Nude Rat" mice were purchased from Vital River (Beijing) Co. Ltd, Beijing, P. R. China. All the mice were 4 week old females. Animal care and experiments were performed in compliance with the relevant laws and in agreement with the guidelines of the Ethics Committee for Animal Experiments of Nankai University.

2.3. Synthesis and of Gd:CdTe QDs

0.2 mmol $CdCl_2$, 0.5×10^{-2} mmol $GdCl_3$ and 1.0 mmol GSH were dissolved in 25.0 mL deionized water in a conical flask. In this step, GSH was employed as the stabilizer to prepare the Gd:CdTe QDs. Then, the reaction mixture was stirred for 10 min, and 0.1 mmol Na_2TeO_3 was introduced into the reaction system as the source of Te^{2-}. Afterwards, 0.24 g $NaBH_4$ was added in the reaction mixture as reducing agent under stirring. The above mixture was mixed with 40 mL 80% $N_2H_4 \cdot H_2O$ quickly after the addition of $NaBH_4$. After 4 h of stirring, the Gd:CdTe QDs were obtained. All the reagents were added in the reaction mixture in turn, and all the operation was conducted at room temperature.

Before the further modification and bioapplication, the as-prepared Gd:CdTe QDs were purified by centrifugation at 12 000 rpm from the alkaline reaction mixture, and they were washed by deionized water and ethanol. Afterwards, they were dried at 60 °C in vacuum for 12 h.

2.4. Synthesis of folic acid conjugated Gd:CdTe QDs

An EDC/NHS solution with a molar ratio of FA : EDC : NHS = 1 : 1 : 2.5 was employed to activate the carboxyl groups of FA. After 30 min of activation, purified Gd:CdTe QDs were added into the FA solution. The mixture was allowed to react at room temperature for 12 h, and then the FA conjugated Gd:CdTe QDs (FA-Gd:CdTe QDs) was obtained. The resultant solutions were washed with deionized water and ethanol again for the removal of unreacted chemicals by centrifugation. The as-purified FA-Gd:CdTe QDs were re-dissolved in PBS buffer solution (pH 7.4) for further applications.

2.5. Characterization

Transmission electron microscopy (TEM) image and the energy dispersive X-ray spectroscopy (EDS) pattern of the Gd:CdTe QDs were acquired on a Philips Tecnai G2 F20 S-TWIN transmission electron microscope (Philips, Holland) using 200 kV electron source. Powder X-ray diffraction (XRD) patterns were collected on a Rigaku D/max-2500 X-ray diffractometer (Rigaku, Japan) with Cu Kα radiation. The ratio of Gd to Cd in purified Gd-doped CdTe QDs was obtained on an ICP-9000(N + M) inductively coupled plasma atomic emission spectroscope (ICP-AES) (TJA, America). XPS spectra were recorded using a Kratos Axwas Ultra DLD spectrometer employing a monochromated Al-Ka X-ray source ($h\nu$ = 1486.6 eV), hybrid (magnetic/electrostatic) optics and a multi-channel plate and delay line detector (DLD). All XPS spectra were recorded using an aperture slot of 300 × 700 microns, survey spectra were recorded with a pass energy of

160 eV, and high resolution spectra with a pass energy of 40 eV. Fourier transform infrared (FTIR) spectra (4000–500 cm^{-1}) in KBr were recorded by using a Vector 22 FTIR spectrophotometer (Bruker, Germany).

The absorption spectra of all samples were obtained from a UV-2450 UV-Vis spectrophotometer (Shimadzu, Japan). The fluorescence emission spectra of all samples were performed using an F-4500 fluorescence spectrophotometer (Hitachi, Japan) equipped with a plotter unit and a quartz cell (1 cm × 1 cm). The slit widths of excitation and emission were 5 and 5 nm, respectively. All optical measurements were performed at room temperature under ambient conditions.

The QYs of the Gd:CdTe QDs and the undoped CdTe QDs were measured by a reference method using Rhodamine 6G (QY = 95%) as reference fluorescent dye, and could be calculated according to the following equation:[47,48]

$$\Phi_Q = \Phi_R(A_R/A_Q)(F_Q/F_R)(n_Q/n_R)^2 \quad (1)$$

where Φ, A, F and n are the quantum yield, the absorbance, the corrected emission intensity and the average refractive index of the sample solution, respectively. Subscripts R refers to the reference, and Q refers to the QDs. Gd:CdTe QDs, undoped CdTe QDs and the reference were dissolved separately in deionized water to make up a series of sample solution in different concentrations. Then, we measured the absorbance (A) and the corrected emission intensity (F) of these samples and drew their F–A curves. In formula (1), $n_Q = n_R = n_{water}$; thus, F_R/A_R and F_Q/A_Q can be replaced by the slope of the reference curve (S_R) and the slope of the QDs curve (S_Q), respectively. Therefore, formula (1) can be converted to the following form:

$$\Phi_Q = \Phi_R(S_Q/S_R) \quad (2)$$

Note that formula (2) was used to calculate the QY of the QDs in this work.

2.6. Confocal fluorescence imaging *in vitro*

100 μg mL^{-1} Gd:CdTe QDs and FA-Gd:CdTe QDs were incubated with HepG2 cells for 4 h at 37 °C and with 5% CO_2. After washing with PBS buffer solution three times, the confocal fluorescence images of cells were acquired with a Leica TSC SP8 (Leica, Germany) laser-scanning microscope, excited with 405 nm light.

2.7. Cellular cytotoxicity assay

MTT assay was employed to measure the cellular cytotoxicity *in vitro*. HepG2 cells were cultured in 96-well plates to a density of 5000 cells per well for 24 h at 37 °C with 5% CO_2. FA-Gd:CdTe QDs dissolved in DMEM solutions in different concentrations of 0, 0.01, 0.05, 0.10, 0.50, 1.00 mg mL^{-1} were added to the wells. Then, the cells were incubated for 24 h at 37 °C with 5% CO_2 and washed with medium three times. Next, a new culture medium containing 10% MTT reagent was introduced in the wells for incubating for 4 h. After removing the medium, the purple formazan product was dissolved with DMSO. Finally, the absorbance of formazan was measured by an enzyme-linked immunosorbent assay reader at 570 nm.

2.8. Targeting fluorescence imaging *in vivo*

In this experiment, three female "Balb/c nude" mice are used as the experimental models: mouse A and mouse C are tumor-bearing mice, but mouse B is a normal mouse without the inoculation of any tumor cells. The tumor-bearing mice are obtained by injecting HepG2 cells into their right axillar without any other treatment. Four weeks later, tumors were observed at the injection sites of mouse A and mouse C. Then, Gd:CdTe QDs, FA-Gd:CdTe QDs and FA-Gd:CdTe QDs are injected into mouse A, mouse B and mouse C, respectively, through their eye veins. Two minutes later after the injection of the contrast agents, FL images are acquired using a Xenogen IVIS Lumina II (Xenogen, USA.) animal FL imaging system.

2.9. Paramagnetism characterization and MR imaging *in vivo*

The paramagnetism of the Gd:CdTe QDs was characterized using an EMX-6/1 electron paramagnetic resonance (EPR) spectrometer (Bruker, Germany). The MR images *in vitro* and *in vivo* were acquired using a 3.0 T Siemens MAGNETOM Trio Tim MRI Scanner (Siemens, Germany).

3. Results and discussion

3.1. Synthesis, modification and characterization of Gd:CdTe QDs

The GSH-stabilized Gd:CdTe QDs were fabricated and surface-modified by a room-temperature strategy as illustrated in

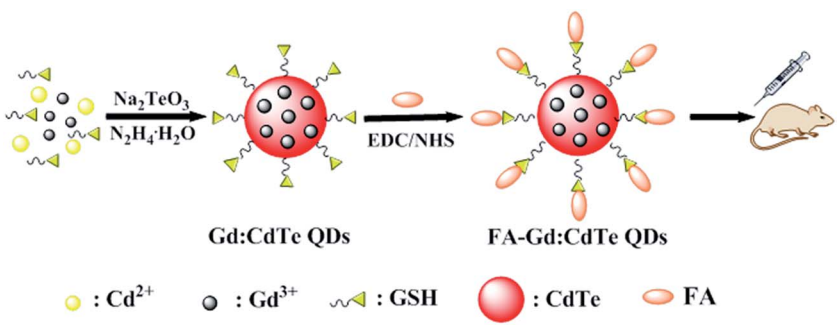

Scheme 1 Schematic protocol for the synthesis of the Gd:CdTe QDs and their surface function with FA.

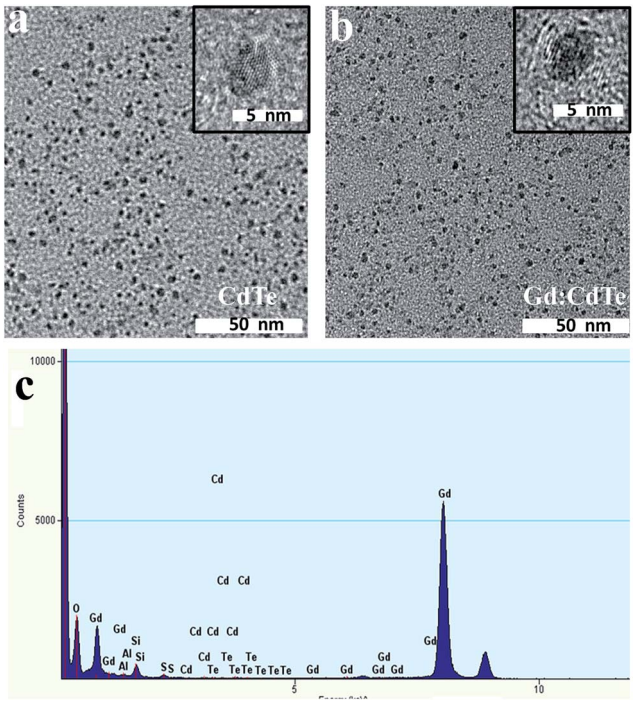

Fig. 1 TEM and HRTEM (inset) images of (a) CdTe QDs and (b) Gd:CdTe QDs. (c) EDS patterns of Gd:CdTe QDs.

Scheme 1. Firstly, $CdCl_2$, $GdCl_3$ and GSH were mixed with deionized water and stirred. Here GSH was employed as the stabilizer for the preparation of the Gd:CdTe QDs. Then, Na_2TeO_3 and $NaBH_4$ were added into the reaction mixture in turn. $NaBH_4$ can reduce the TeO_3^{2-} to Te^{2-}, which is the precursor for combining with Cd^{2+} and Gd^{3+} to fabricate the Gd:CdTe QDs. After the addition of $NaBH_4$, the above mixture was mixed with $N_2H_4 \cdot H_2O$, which not only affords an alkaline condition for the reaction system, but also replaces N_2 as the protector to avoid the oxidation of Te^{2-} precursor.[6,49] After 4 h of stirring at room temperature, the Gd:CdTe QDs were established, and then they were conjugated with FA through an EDC/NHS coupling route.[45,46] The obtained FA-Gd:CdTe QDs were employed in the tumor-targeted imaging applications since FA is a typical targeting molecule to discern cancer cells.[46]

In this study, we used TEM to characterize the particle size and morphology of the Gd:CdTe QDs. Compared to the undoped CdTe QDs, the as-prepared Gd:CdTe QDs are quasi-spherical particles with uniform distribution of particle size (Fig. 1a and b). As shown in the insets of Fig. 1a and b, the HRTEM images demonstrate that both the Gd-doped and undoped CdTe QDs have the same shape and particle diameter of approximately 3 nm. The composition of the Gd:CdTe QDs is qualitatively measured by EDS spectrum (Fig. 1c) and XPS spectra (Fig. 2). The EDS pattern confirms the presence of the Gd element in the as-prepared Gd:CdTe QDs. As shown in Fig. 2, the characteristic peaks of Gd 4d, Cd $3d_{5/2}$, Cd $3d_{3/2}$, Te $3d_{5/2}$ and Te $3d_{3/2}$ were observed at 151.8 eV, 403.2 eV, 410.0 eV, 570.2 eV and at 581.0 eV in the XPS spectra, respectively. These results indicate that the as-prepared Gd:CdTe QDs are composed of Cd, Te and Gd, and the dopant (Gd^{3+}) has been successfully introduced into the CdTe QDs. For quantitative characterization, the result of ICP-AES certificated that the molar–molar ratio of Gd element to Cd element in the QDs is 2.03%.

XRD spectrum is used to reveal the crystal structure of the as-prepared QDs. As shown in Fig. 3a, the reflection peaks in the patterns of Gd:CdTe QDs and original CdTe QDs are located at the same position without the appearance of any other impurity peaks, which indicates that the two samples have a similar zinc blende structure. This indicates that the incorporation of the impurities does not change the lattice structure of the Gd:CdTe QDs compared with the host CdTe QDs. It was observed in

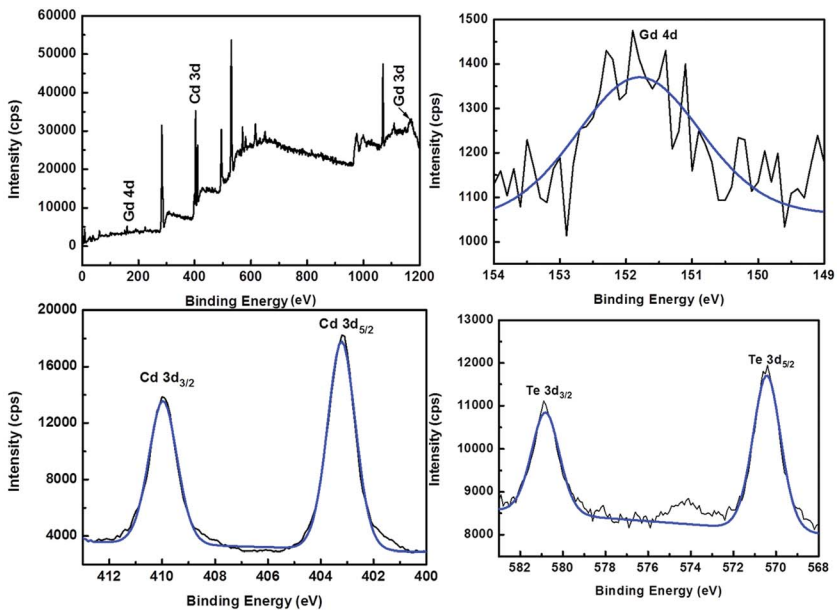

Fig. 2 XPS spectra of the as-prepared Gd:CdTe. (a) XPS survey spectrum, (b) binding energy spectrum of Gd 4d, (c) binding energy spectrum of Cd $3d_{3/2}$ and $3d_{5/2}$; (d) binding energy spectrum of Te $3d_{3/2}$ and $3d_{5/2}$.

Fig. 3a that the diffraction peaks of Gd-doped CdTe QDs were slightly shifted toward the low angle area compared with the XRD diffraction peaks of undoped CdTe QDs, which confirmed that the doped Gd^{3+} ions have been embedded into the crystal lattice of CdTe QDs. This result illustrates that the distance of the ions in the lattice of the doped QDs was increased due to the replacement of larger Cd^{2+} ions by the smaller Gd^{3+} ions in the CdTe QDs lattice.

The FTIR spectra of FA, Gd:CdTe QDs and FA-Gd:CdTe QDs were used to confirm the conjugation of FA with the QDs. As shown in Fig. 3b, after conjugation with FA, the FA-Gd:CdTe QDs has a new absorption peak at 1481 cm^{-1} comparing with the unconjugated Gd:CdTe QDs, which is assigned to the stretching vibration of the phenyl. Phenyl is the characteristic ligand of FA, and its absorption peak is also observed on the FTIR spectrum of FA. This result indicates that the FA has been successfully conjugated with the CdTe QDs. In addition, we noticed that the characteristic absorption peaks at 1698 and 3497 cm^{-1} resulting from the C=O vibration of FA-Gd:CdTe QDs are slighter than those of FA, and these peaks are absent on the spectrum of Gd:CdTe QDs. This illustrates that the carboxyl of FA has reacted with the amino group of GSH, and FA was conjugated on the surface of the CdTe QDs.

3.2. Optical properties

The absorption (Abs) and fluorescence (FL) emission spectra of the undoped and Gd-doped CdTe QDs are revealed in Fig. 4a. Compared with the undoped CdTe QDs, there is a slight blue-shift on the Abs spectrum of Gd:CdTe QDs. This indicates that the particle size of the QDs decreased somewhat when the dopant was introduced into it, which might be attributed to the ionic radius difference between Cd^{2+} and Gd^{3+}. As shown in Fig. 4a, the FL spectra illustrate that both the Gd-doped and undoped CdTe QDs have sharp and narrow emission peaks at 640 nm, but the FL intensity of Gd:CdTe QDs is weaker than that of the undoped CdTe QDs due to the quenching of Gd^{3+} ions.[7] It is also observed that there is a bright red color emitted from the Gd:CdTe QDs with the irradiation by a 365 nm UV lamp (the inset in Fig. 4a). Fig. 4b shows the F–A curves and the slope of Rh6G, undoped and Gd-doped CdTe QDs. According to formula (2), the QY of the undoped and Gd-doped CdTe QDs are calculated to be 38% and 37%, respectively.

The result of QY survey demonstrates that the QY of the Gd:CdTe QDs slightly decreased when the dopant ions were introduced into the CdTe QDs. Therefore, to choose the optimum synthesis ratios of the reactants, including Gd^{3+} ions, GSH, Na_2TeO_3 and $N_2H_4 \cdot H_2O$, several further studies were investigated (Fig. 5). As shown in Fig. 5a, the FL intensity of the Gd:CdTe QDs decreased with the increase of the dopant. Because the ionic radius of Gd^{3+} is less than that of Cd^{2+}, the surface defect of the doped QDs was increased by the difference of the cations when Gd^{3+} was doped into the QDs. As a result,

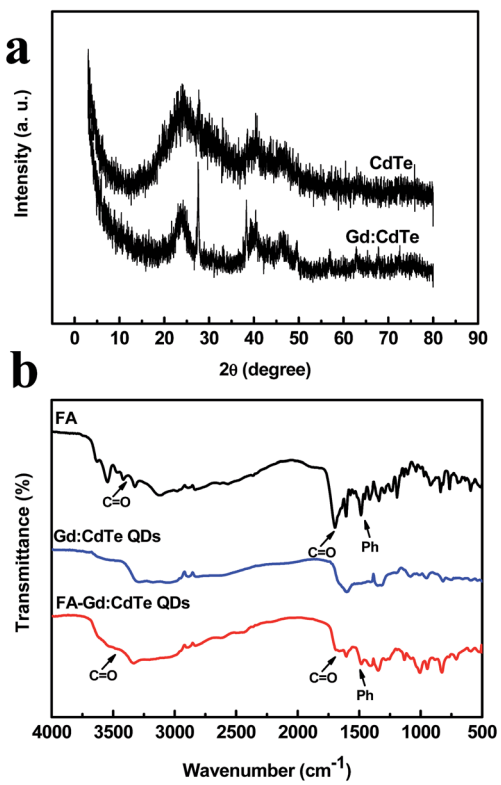

Fig. 3 (a) XRD patterns of CdTe QDs and Gd:CdTe QDs. (b) FTIR spectra of FA, Gd:CdTe QDs and FA-Gd:CdTe QDs.

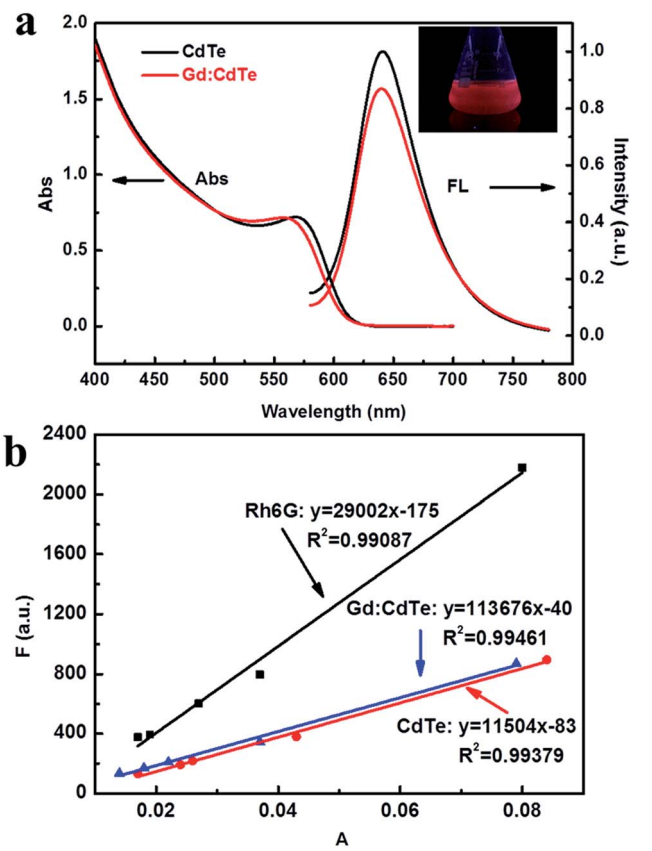

Fig. 4 (a) Abs and FL spectra of the undoped and Gd-doped CdTe QDs. The inset: FL image of the Gd:CdTe QDs irradiation by a 365 nm UV lamp. (b) F–A curves of the undoped and Gd-doped CdTe QDs.

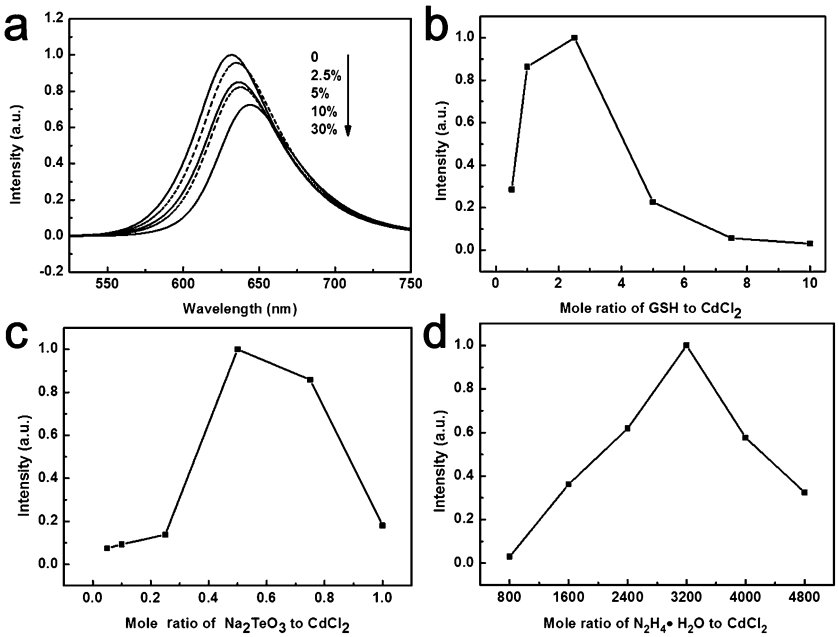

Fig. 5 (a) The FL spectra of Gd:CdTe QDS with different Gd : Cd mol ratios. (b–d) The FL intensity of Gd:CdTe QDS with different GSH : $CdCl_2$, Na_2TeO_3 : $CdCl_2$ and $N_2H_4 \cdot H_2O$: $CdCl_2$ molar ratios.

the excessive Gd^{3+} dopant can quench the fluorescence of the Gd-doped QDs. The FL intensity of the Gd-doped CdTe QDs declines 20% and 40% compared with that of the bulk CdTe QDs when the addition of the dopant Gd reaches 5% and 30% (molar–molar ratio, contrast to Cd in the QDs), respectively. Since the longitudinal relaxation rate (r_1) is proportional to the content of the Gd element in the Gd based MR imaging agents,[8] 2.5% is chosen as the optimum dopant ratio owing to its contribution for both novel FL intensity and magnetic capability.

GSH plays an important role in the synthesis of Gd:CdTe QDs. It can increase the stability and reduce the surface defect of the doped QDs. However, excess GSH might quench the fluorescence of the QDs owing to their considerable steric effect. Therefore, when we increase the density of GSH, it increased to the highest point with increase in these three reactants' mole ratio to Cd^{2+} in the QDs, and then it decreased (Fig. 5b). Furthermore, the increasing of Te^{2-} can reduce the free Cd^{2+} ions in the reaction solution, which can coordinate with GSH, then increase the density of the stabilizer. QDs are usually synthesized in alkaline conditions, the increase in N_2H_4 can enhance the alkalinity of the reaction system and the stability of the QDs. However, excess N_2H_4 reduces the density of the GSH by reacting with the carboxyl of GSH, which increased the surface defect of the QDs. Therefore, when we increased the ratio of Na_2TeO_3 and N_2H_4, the influence on the FL intensity of the doped QDs was same as that by enhancing the ratio of GSH. These results have been supported by Fig. 5c and d.

Because these reactants gave non-contribution to the magnetic capability of the Gd:CdTe QDs, the FL intensity became the only standard to determine the optimum reactant ratios for the synthesis of the Gd:CdTe QDs. According to the experimental results revealed in Fig. 5, the optimum molar ratio of Gd : Cd : Na_2TeO_3 : $N_2H_4 \cdot H_2O$ is 0.025 : 1 : 0.5 : 3200.

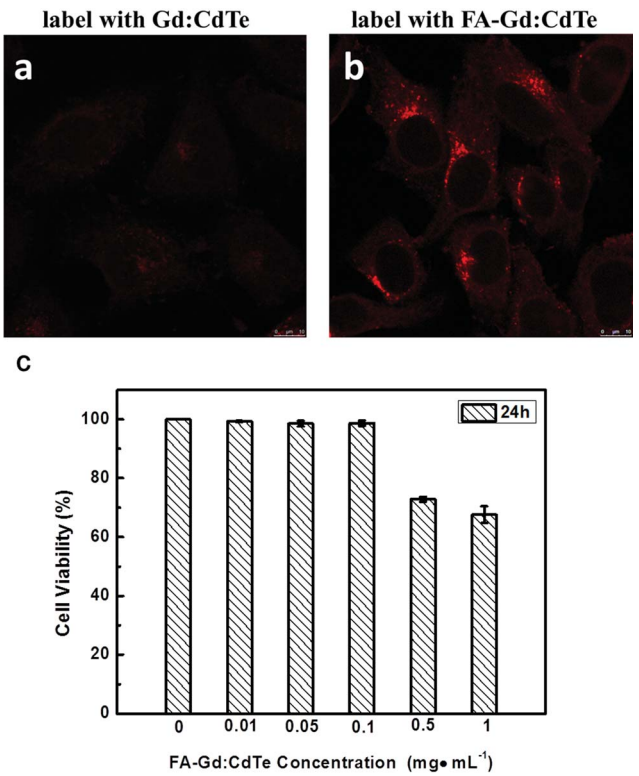

Fig. 6 The fluorescence images of the HepG2 cells labeled with (a) Gd:CdTe QD and (b) FA-Gd:CdTe QDs, (c) Effect of FA-Gd:CdTe QDs on the viability of HepG2 cells measured by MTT assay.

3.3. Cellular fluorescence imaging in HepG2 cells

In this study, HepG2 cells (a type of human liver cancer cell) were chosen as a model to confirm the targeting imaging ability of the as-prepared FA-Gd:CdTe QDs due to their high expression of FA acceptor, a target which can combine with FA.[50,51]

The images are acquired using a confocal laser scanning microscope. As shown in Fig. 6, the HepG2 cells treated with FA-Gd:CdTe QDs exhibited bright red fluorescence, which is much brighter than the fluorescence emitted from the cells labelled with Gd:CdTe QDs (Fig. 6a and b). This suggests that the as-designed FA-Gd:CdTe QDs are successful agents for targeting cellular FL imaging *in vitro*.

The cytotoxicity of the FA-Gd:CdTe QDs is further investigated using MTT (methyl thiazolyl tetrazolium) assay associated with HepG2 cells. As shown in Fig. 6c, it illustrates that the cell viability of HepG2 cells remains more than 80% until the concentration of the agents reaches 0.5 mg mL^{-1}. This result reveals that the FA-Gd:CdTe QDs have non-evidence cytotoxicity to HepG2 cells, which is attributed to the protection of the non-toxic GSH stabilizer coupled at the surface of the Gd:CdTe QDs.[52]

3.4. Tumor-targeted fluorescence imaging application *in vivo*

The low-toxicity FA-Gd:CdTe QDs also exhibits excellent targeting imaging capability for FL imaging application *in vivo*. In this experiment, three female "Balb/c" nude mice are used as the experimental models: mouse A and mouse C are tumor-bearing mice, but mouse B is a normal mouse without the inoculation of any tumor cells. The tumor-bearing mice are obtained by injecting HepG2 cells into their right axillar without any other treatment. Four weeks later, tumors were observed at the injection sites of mouse A and mouse C. Then, Gd:CdTe QDs, FA-Gd:CdTe QDs and FA-Gd:CdTe QDs are injected into mouse A, mouse B and mouse C, respectively, through their eye veins. Two minutes later after the injection of the contrast agents, FL images are acquired using an animal FL imaging system. As shown in Fig. 7a and b, there are significant signals on the brains of both mouse A and mouse B. However, no signal can be observed from the tumor site of either mouse A or mouse B. Furthermore, it can observe significant FL signal from the tumor site in mouse C, and there is very low signal from its brain (Fig. 7c). 90 min later, non-evident FL signal can be perceived from these three mice, which shows that the two agents can be quickly cleared from the body of the mice with blood circulation. These results suggest that the as-designed FA-Gd:CdTe QDs have excellent targeting FL imaging capability in a live animal model, and they can be employed as a successful targeting FL imaging agent *in vivo*.

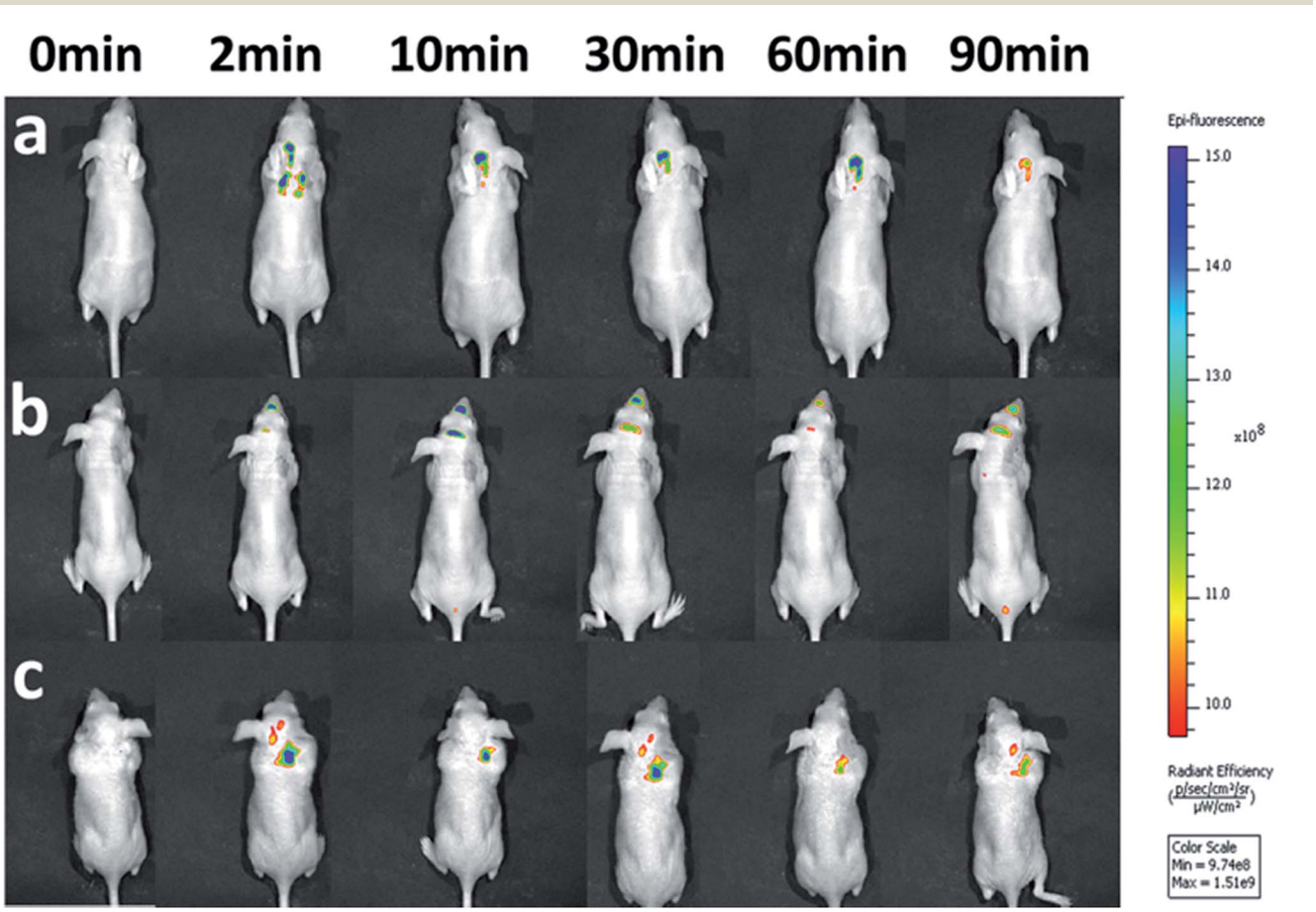

Fig. 7 (a) FL images of the mouse with tumor labelled by Gd:CdTe QDs. (b) FL images of normal mouse labelled by FA-Gd:CdTe QDs. (c) FL images of the mouse with tumor labelled by FA-Gd:CdTe QDs.

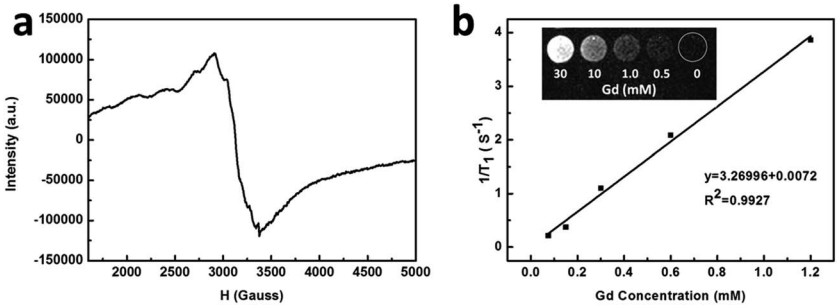

Fig. 8 (a) EPR spectrum of Gd:CdTe QDs. (b) Longitudinal relaxation rate r_1 *versus* different molar concentrations of Gd:CdTe QDs, inset: T_1-weighted MR images of Gd:CdTe QDs at different Gd concentrations.

3.5. MR imaging application *in vivo*

As a FL/MR dual-modal imaging contrast agent, Gd:CdTe QDs simultaneously have outstanding magnetic properties, in addition to high quality optical properties. The magnetic properties of the QDs and T_1-weighted MR images are measured with an electron paramagnetic resonance (EPR) spectrometer and a 3.0 T clinical MRI instrument. The EPR spectrum affords an excellent suggestion of the paramagnetism of the Gd:CdTe QDs (Fig. 8a). It is also demonstrated that the T_1-weighted MR signal of the Gd:CdTe QDs will be enhanced with increase in the concentration of the Gd agent in water (the inset of Fig. 8b), and the longitudinal relaxation rate of the Gd:CdTe QDs is 3.27 mM^{-1} s^{-1} (Fig. 8b), which is approximately equivalent compared with that of Omniscan, one of the most frequently used commercial MRI contrast agents.[20,23] For *in vivo* MR imaging, the FA-Gd:CdTe QDs is dissolved in PBS buffer solution (pH 7.4) and injected into a tumor-bearing "Nude Rat" mouse.

Fig. 9a and b exhibit the MR images of the tumor-bearing mouse before and 20 min after the injection with a 3.0 T MR human clinical scanner. This illustrated that the MR signal of the tumor site was much higher after the injection of the targeted probe (Fig. 9). All the above results show that the as-prepared FA-Gd:CdTe QDs is a suitable agent for targeting MR imaging *in vivo*.

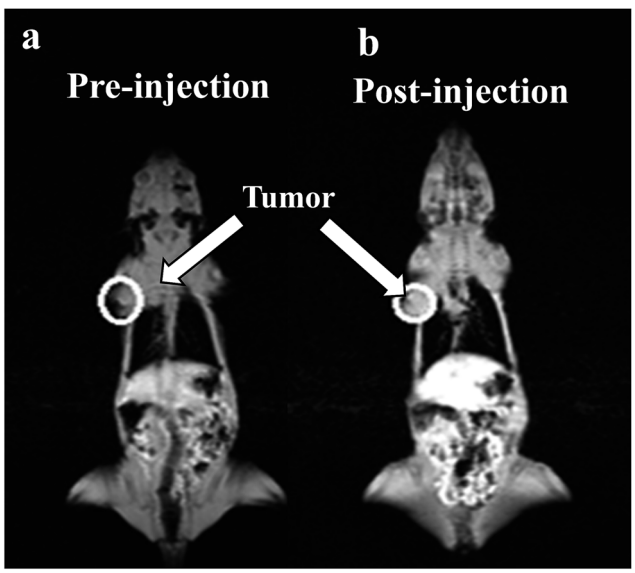

Fig. 9 T_1-weighted MR images of a tumor-bearing "Nude rat" before (a) and after (b) injection of the agent.

4. Conclusion

In conclusion, we prepared Gd-doped CdTe with ultrasmall particle size, high QY, excellent aqueous solubility and biocompatibility for targeting FI/MRI dual-modal imaging both *in vitro* and *in vivo*. The Gd:CdTe QDs are synthesized using a facile room-temperature approach in aqueous solution directly. The Gd:CdTe QDs exhibit low toxicity toward cells and outstanding magnetic properties, and they are employed in cellular FL imaging, FL and MR imaging *in vivo* as the tumor-targeted agent successfully.

Acknowledgements

This work was supported by the National Basic Research Program of China (973 Program) (nos 2011CB707703 and 2012CB910601), the National Natural Science Foundation of China (nos 21075069 and 21275078), and the Tianjin Natural Science Foundation (no. 11JCZDJC21700).

References

1 A. P. Alivisatos, *Science*, 1996, **271**, 933–937.
2 M. Bruchez, M. Moronne, P. Gin, S. Weiss and A. P. Alivisatos, *Science*, 1998, **281**, 2013–2016.
3 W. Cai and X. Chen, *Small*, 2007, **3**, 1840–1854.
4 X. Michalet, F. F. Pinaud, L. A. Bentolila, J. M. Tsay, S. Doose, J. J. Li, G. Sundaresan, A. M. Wu, S. S. Gambhir and S. Weiss, *Science*, 2005, **307**, 538–544.
5 H. S. Mansur, *Wiley Interdiscip. Rev.: Nanomed. Nanobiotechnol.*, 2010, **2**, 113–129.
6 D. Zhou, M. Lin, Z. Chen, H. Sun, H. Zhang, H. Sun and B. Yang, *Chem. Mater.*, 2011, **23**, 4857–4862.
7 Y. Liu, K. Ai, Q. Yuan and L. Lu, *Biomaterials*, 2011, **32**, 1185–1192.

8 R. Koole, W. J. M. Mulder, M. M. Van Schooneveld, G. J. Strijkers, A. Meijerink and K. Nicolay, *Wiley Interdiscip. Rev.: Nanomed. Nanobiotechnol.*, 2009, **1**, 475–491.
9 P. Shao, Q. Zhang, Y. Li and H. Wang, *J. Mater. Chem.*, 2011, **21**, 151–156.
10 G. Hong, J. T. Robinson, Y. Zhang, S. Diao, A. L. Antaris, Q. Wang and H. Dai, *Angew. Chem., Int. Ed.*, 2012, **51**, 9818–9821.
11 H. Kobayashi, M. Ogawa, R. Alford, P. L. Choyke and Y. Urano, *Chem. Rev.*, 2009, **110**, 2620–2640.
12 M. J. Ruedas-Rama, J. D. Walters, A. Orte and E. A. H. Hall, *Anal. Chim. Acta*, 2012, **751**, 1–23.
13 N. Singh, S. Charan, K. Sanjiv, S. H. Huang, Y. C. Hsiao, C. W. Kuo, F. C. Chien, T. C. Lee and P. Chen, *Bioconjugate Chem.*, 2012, **23**, 421–430.
14 N. Pradhan, D. Goorskey, J. Thessing and X. Peng, *J. Am. Chem. Soc.*, 2005, **127**, 17586–17587.
15 J. Cheon and J.-H. Lee, *Acc. Chem. Res.*, 2008, **41**, 1630–1640.
16 Y. Liu, K. Ai, J. Liu, Q. Yuan, Y. He and L. Lu, *Angew. Chem., Int. Ed.*, 2012, **51**, 1437–1442.
17 S. Zeng, M. K. Tsang, C. F. Chan, K. L. Wong and J. Hao, *Biomaterials*, 2012, **33**, 9232–9238.
18 Z. Li, S. Yin, L. Cheng, K. Yang, Y. Li and Z. Liu, *Adv. Funct. Mater.*, 2014, **24**, 2312–2321.
19 G. Liang, D. Ye, X. Zhang, F. Dong, H. Chen, S. Zhang, J. Li, X. Shen and J. Kong, *J. Mater. Chem. B*, 2013, **1**, 3545–3552.
20 D.-H. Hu, Z. H. Sheng, P. F. Zhang, D. Z. Yang, S. H. Liu, P. Gong, D. Y. Gao, S. T. Fang, Y. F. Ma and L. T. Cai, *Nanoscale*, 2013, **5**, 1624–1628.
21 W. Fan, B. Shen, W. Bu, F. Chen, K. Zhao, S. Zhang, L. Zhou, W. Peng, Q. Xiao, H. Xing, J. Liu, D. Ni, Q. He and J. Shi, *J. Am. Chem. Soc.*, 2013, **135**, 6494–6503.
22 A. K. Saha, P. Sharma, H. B. Sohn, S. Ghosh, R. K. Das, A. F. Hebard, H. Zeng, C. Baligand, G. A. Walter and B. M. Moudgil, *J. Mater. Chem. B*, 2013, **1**, 6312–6320.
23 A. Louie, *Chem. Rev.*, 2010, **110**, 3146–3195.
24 I. F. Li and C. S. Yeh, *J. Mater. Chem.*, 2010, **20**, 2079–2081.
25 J. Cheon and J. H. Lee, *Acc. Chem. Res.*, 2008, **41**, 1630–1640.
26 W. R. Algar, K. Susumu, J. B. Delehanty and I. L. Medintz, *Anal. Chem.*, 2011, **83**, 8826–8837.
27 J. H. Gao, H. W. Gu and B. Xu, *Acc. Chem. Res.*, 2009, **42**, 1097–1107.
28 A. Louie, *Chem. Rev.*, 2010, **110**, 3146–3195.
29 J. Key and J. F. Leary, *Int. J. Nanomed.*, 2014, **9**, 711–726.
30 F. F. Wang, X. J. Yang, L. Ma, B. R. Huang, N. Na, Y. E, D. C. He and J. Ouyang, *J. Mater. Chem.*, 2012, **22**, 24597–24604.
31 S. Lee, J. Xie and X. Y. Chen, *Chem. Rev.*, 2010, **110**, 3087–3111.
32 H. S. Choi, W. Liu, F. Liu, K. Nasr, P. Misra, M. G. Bawendi and J. V. Frangioni, *Nat. Nanotechnol.*, 2010, **5**, 42–47.
33 Z. Liu, F. Pu, S. Huang, Q. Yuan, J. Ren and X. Qu, *Biomaterials*, 2013, **34**, 1712–1721.
34 A. A. Bol and A. Meijerink, *Phys. Rev. B: Condens. Matter Mater. Phys.*, 1998, **58**, 15997–16000.
35 N. Murase, R. Jagannathan, Y. Kanematsu, M. Watanabe, A. Kurita, K. Hirata, T. Yazawa and T. Kushida, *J. Phys. Chem. B*, 1999, **103**, 754–760.
36 W. W. Zhang and G. F. Strouse, *J. Am. Chem. Soc.*, 2011, **133**, 7482–7489.
37 S. Santra, H. S. Yang, P. H. Holloway, J. T. Stanley and R. A. Mericle, *J. Am. Chem. Soc.*, 2005, **127**, 1656–1657.
38 S. Kar, W. L. Boncher, D. Olszewski, N. Dollahon, R. Ash and S. L. Stoll, *J. Am. Chem. Soc.*, 2010, **132**, 13960–13962.
39 F. Zhang, X. W. He, W. Y. Li and Y. K. Zhang, *J. Mater. Chem.*, 2012, **22**, 22250–22257.
40 A. Signore, S. J. Mather, G. Piaggio, G. Malviya and R. A. Dierckx, *Chem. Rev.*, 2010, **110**, 3112–3145.
41 Y. L. Dai, H. H. Xiao, J. H. Liu, Q. H. Yuan, P. A. Ma, D. M. Yang, C. X. Li, Z. Y. Cheng, Z. Y. Hou, P. P. Yang and J. Lin, *J. Am. Chem. Soc.*, 2013, **135**, 18920–18929.
42 M. Pokhrel, L. C. Mimun, B. Yust, G. A. Kumar, A. Dhanale, L. Tang and D. K. Sardar, *Nanoscale*, 2014, **6**, 1667–1674.
43 J. Kim, Y. Piao and T. Hyeon, *Chem. Soc. Rev.*, 2009, **38**, 372–390.
44 L. W. Liu, W. C. Law, K. T. Yong, I. Roy, H. Ding, F. Erogbogbo, X. H. Zhang and P. N. Prasad, *Analyst*, 2011, **136**, 1881–1886.
45 Z. Zhou, C. Zhang, Q. Qian, J. Ma, P. Huang, X. zhang, L. Pan, G. Gao, H. Fu, S. Fu, H. Song, X. Zhi, J. Ni and D. Cui, *J. Nanobiotechnol.*, 2013, **11**, 17.
46 J. B. Ma, P. Huang, M. He, L. Y. Pan, Z. J. Zhou, L. L. Peng, G. Gao and D. X. Cui, *J. Phys. Chem. B*, 2012, **116**, 14062–14070.
47 J. N. Demas and G. A. Crosby, *J. Phys. Chem.*, 1971, **75**, 991–1024.
48 A. T. R. Williams, A. S. Winfield and J. N. Miller, *Analyst*, 1983, **108**, 1067–1071.
49 D. Zhou, J. Han, Y. liu, M. Liu, X. Zhang, H. Zhang and B. Yang, *J. Phys. Chem. C*, 2010, **114**, 22487–22492.
50 Y. Zhang, J. M. Liu and X. P. Yan, *Anal. Chem.*, 2012, **85**, 228–234.
51 Q. Yin, F. Y. Yap, L. C. Yin, L. Ma, Q. Zhou, L. W. Dobrucki, T. M. Fan, R. C. Gaba and J. J. Cheng, *J. Am. Chem. Soc.*, 2013, **135**, 13620–13623.
52 C. Xue, W. Liu, J. Wu, X. Yang and H. Xu, *Toxicol. In Vitro*, 2011, **25**, 110–116.